Coordination Chemistry Reviews 254 (2010) 2623–2633

Contents lists available at ScienceDirect

Coordination Chemistry Reviews

journal homepage: www.elsevier.com/locate/ccr

Review

Lanthanide luminescence efficiency in eight- and nine-coordinate complexes: Role of the radiative lifetime

Jean-Claude G. Bünzli[a,b,*], Anne-Sophie Chauvin[a], Hwan Kyu Kim[b], Emmanuel Deiters[a], Svetlana V. Eliseeva[a]

[a] Laboratory of Lanthanide Supramolecular Chemistry, École Polytechnique Fédérale de Lausanne, BCH 1402, CH-1015 Lausanne, Switzerland
[b] WCU Center for Next Generation Photovoltaic Systems, Korea University, Sejong Campus, Jochiwon, ChungNam 339-700, South Korea

Contents

ARTICLE INFO

Article history:
Received 7 January 2010
Accepted 3 April 2010
Available online 14 April 2010

Keywords:
Lanthanide
Luminescence
Nine-coordination
Eight-coordination
Mononuclear
Binuclear
Helicate
Radiative lifetime
Quantum yield
Sensitization efficiency

ABSTRACT

The photophysical parameters for the sensitization of metal-centred luminescence are analyzed in two series of complexes with tridentate and hexadentate ligands having N_xO_y chelating units. In particular, the radiative lifetime τ_{rad} is experimentally estimated for 29 nine-coordinate Eu^{III} complexes and 10 eight- and nine-coordinate Yb^{III} complexes. The known dependence of τ_{rad} on refractive index is substantiated by comparing data for solid-state samples and solutions. Moreover, a clear dependence of τ_{rad} with the coordination environment is evidenced and in the case of Eu^{III}, a comparison between τ_{rad} and the nephelauxetic effect generated by the ligands is attempted. Altogether, this extensive analysis points to the importance of having a handle on τ_{rad} when designing ligands for highly luminescent lanthanide-containing molecular edifices. This, in turn, should stimulate initiating theoretical considerations to unravel a reliable relationship between τ_{rad} and the electronic structure of the ligands.

1. Luminescence of lanthanide complexes

The richness and complexity of lanthanide optical spectra has fascinated chemists since the 1880s when renowned scientists such as Sir William Crookes, LeCoq de Boisbaudran, Eugène Demarçay or, later, Georges Urbain, the discoverer of the highly emissive Y_2O_3:Eu phosphor, were using luminescence as an analytical tool to test the purity of their samples and to identify potential new elements. Soon, optical glasses, filters, and lasers benefitted from the sharp and characteristic 4f–4f absorption and emission bands. In the mid 1970s E. Soini and I. Hemmilä proposed lanthanide luminescent probes for time-resolved immunoassays and this has been the starting point of the current numerous bio-applications based on optical properties of lanthanides. Presently, trivalent

* Corresponding author at: Laboratory of Lanthanide Supramolecular Chemistry, École Polytechnique Fédérale de Lausanne, BCH 1402, CH-1015 Lausanne, Switzerland. Tel.: +41 216939821; fax: +41 216939825.
E-mail address: jean-claude.bunzli@epfl.ch (J.-C.G. Bünzli).

0010-8545/$ – see front matter © 2010 Elsevier B.V. All rights reserved.
doi:10.1016/j.ccr.2010.04.002

lanthanide (Ln^{III}) complexes are ubiquitous luminescent tags for bio-analytical applications [1] and serve as light-emitting materials in numerous optical and lighting devices [2]. Their line-like emission spectra span the entire visible and near-infrared (NIR) ranges, and long excited state lifetimes allow facile time-resolved detection.

With the exception of La^{III} and Lu^{III}, all of trivalent ions are luminescent; Gd^{III} emits in the UV (312–315 nm); typically, Pr^{III}, Sm^{III}, Eu^{III}, Tb^{III}, Dy^{III}, and Tm^{III} display visible luminescence while ions such as Nd^{III}, Ho^{III}, Er^{III}, or Yb^{III} have NIR luminescence. Several ions emit in the visible and/or NIR ranges, depending on their coordination environment. Some ions are fluorescent ($\Delta S = 0$), others are phosphorescent ($\Delta S > 0$), and some are both. The sharpness of the emission lines results from the shielding of the 4f orbitals by the $5s^2 5p^6$ filled sub-shells so that reorganization consecutive to excitation of an electron into a 4f level of higher energy does not greatly influence the bonding strength in the molecule. Consequently, the Stokes' shift is very small when excitation is achieved directly into the 4f levels. Electric dipole (ED) f–f transitions are forbidden by Laporte's rule while the much less intense magnetic dipole (MD) transitions are allowed. As a result of *J*-mixing and of the admixture of vibrational states and/or states from the surrounding ligands into 4f orbitals, ED transitions are detected with intensity of the same order of magnitude as MD transitions, with the exception of some so-called "hypersensitive" or "induced electric dipole" transitions which may be an order of magnitude more intense. Selection rules governing these transitions exist for every quantum number (S, L, J) as well as for the symmetry point group of the metal environment. These aspects are well known [3] and have been presented in recent reviews [4,5].

Important parameters characterizing the emission of light from an excited state are the quantum yield *Q*, which is equal to the ratio between the number of emitted photons divided by the number of absorbed photons, and the lifetime of the excited state $\tau_{obs} = 1/k_{obs}$ with k_{obs} being the rate constant for de-population of the excited state. If the metal ion is directly excited into a 4f level, these two quantities are related by:

$$Q_{Ln}^{Ln} = \frac{k_{rad}}{k_{obs}} = \frac{\tau_{obs}}{\tau_{rad}} \tag{1}$$

where k_{rad} is the radiative rate constant; the *intrinsic quantum yield* Q_{Ln}^{Ln} reflects the extent of non-radiative deactivation processes occurring through interactions with the surroundings of the metal ion; finally, the observed rate constant k_{obs} is the sum of the deactivation rates:

$$k_{obs} = k_{rad} + \sum_n k_n^{nr} = k_{rad} + \sum_i k_i^{vibr}(T) + \sum_j k_j^{pet}(T) + \sum_k k'^{nr}_k \tag{2}$$

in which k^{nr} are the non-radiative rate constants; the superscript *vibr* points to vibration-induced processes while *pet* refers to photo-induced electron transfer de-activations, e.g. caused by LMCT states; the rate constants k' are associated with the remaining deactivation paths. The intrinsic quantum yield essentially depends on the energy gap ΔE between the emissive state of the metal ion and the highest sub-level of its ground, or receiving, multiplet. The smaller this gap, the easier is its matching by non-radiative deactivation processes. As a rule of thumb, it is recommended to adjust the largest phonon energy in the metal–ion environment so that it is equal or greater than $\Delta E/6$.

In the absence of non-radiative deactivation processes, $k_{obs} = k_{rad}$ and the quantum yield is equal to 1, which seldom happens. In the case of Eu^{III} for instance, inorganic phosphors such as Y_2O_3:Eu have quantum yields close to unity (95–99% depending on the doping rate) [6] while the largest quantum yield reported for a complex with organic ligands, [Eu(tta)$_3$DBSO] (tta is thenoyltrifluoroacetylacetonate and DBSO dibenzylsulfoxide) is 85% [7]. In fact, complexes considered to be highly luminescent have quantum yields in the range 50–70% [8–10] and this figure is difficult to improve. These data are determined by excitation into the ligand levels (or into the charge-transfer band for the inorganic phosphors) and are termed *overall quantum* yields:

$$Q_{Ln}^{L} = \eta_{sens} \times Q_{Ln}^{Ln} \tag{3}$$

In this expression, η_{sens} is the *sensitization efficiency* defined as the efficacy with which energy is transferred from the feeding levels of the ligands onto the Ln^{III} excited states. When the complex is excited into the ligand levels, the apparent Stokes' shift is very large, which represents a definite advantage when lanthanide ions are used as bio-probes. Determination of the sensitization efficiency requires the knowledge of both overall and intrinsic quantum yields. However, experimental determination of the intrinsic quantum yield is difficult in view of the faint absorbance of f–f transitions so that this quantity is very often calculated from Eq. (1) which, in turn, requires evaluation of the radiative lifetime. This parameter can in principle be retrieved from the absorption spectrum $\varepsilon(\tilde{\nu})$ using Einstein's rates of spontaneous emission *A* from an initial state $|\Psi_J\rangle$ to a final state $|\Psi'_{J'}\rangle$ defined by quantum numbers S, L, J and S′, L′, J′, respectively:

$$A(\Psi_J, \Psi'_{J'}) = k_{rad} = \frac{1}{\tau_{rad}} = \frac{64\pi^4 \tilde{\nu}_{mean}^3}{3h(2J+1)} \left[\frac{n(n^2+2)^2}{9} D_{ED} + n^3 D_{MD} \right] \tag{4}$$

$$\tilde{\nu}_{mean} = \frac{\int \tilde{\nu} \cdot \varepsilon(\tilde{\nu}) d\tilde{\nu}}{\int \varepsilon(\tilde{\nu}) d\tilde{\nu}} \tag{5}$$

$\tilde{\nu}_{mean}$ is the mean energy of the transition, *h* Planck's constant, and *n* the refractive index; D_{ED} and D_{MD} are given by the following equations:

$$D_{ED} = e^2 \cdot \sum_{\lambda=2,4,6} \Omega_\lambda \cdot \left| \left\langle \Psi_J \left\| U^\lambda \right\| \Psi_{J'} \right\rangle \right|^2 \tag{6}$$

$$D_{MD} = \left(\frac{e \cdot h}{4 \cdot \pi \cdot m_e \cdot c} \right)^2 \cdot \left| \left\langle \Psi_J \right| \left| L + 2S \right| \left| \Psi_{J'} \right\rangle \right|^2 \tag{7}$$

e, m_e, *h*, and *c* are the electron charge and mass, Planck's constant and the velocity of light *in vacuo*. The three phenomenological Judd-Ofelt parameters Ω_λ (in cm^2) [4] can be calculated from the f–f absorption spectrum. The squared bracketed expressions are dimensionless doubly reduced matrix elements which are insensitive to the metal environment and which are tabulated [11]. However, except in few cases, this calculation is not trivial and large errors may occur, particularly for ions for which Judd-Ofelt theory does not apply well. Fortunately, there is a way out in some cases. For instance, if the absorption spectrum to the emissive level is known, which may be the case when the luminescence transitions terminate onto the ground level, the radiative lifetime can be extracted from the following equation (N_A is Avogadro's number):

$$\frac{1}{\tau_{rad}} = 2303 \times \frac{8\pi c n^2 \tilde{\nu}^2 (2J+1)}{N_A (2J'+1)} \int \varepsilon(\tilde{\nu}) d\tilde{\nu} \tag{8}$$

where *J* refers to the ground state and *J′* to the excited state.

In this paper, we will be discussing τ_{rad} values for the Yb($^2F_{5/2}$) state obtained in this way since molar absorption coefficients for the Yb($^2F_{5/2} \leftarrow {}^2F_{7/2}$) transition in complexes with organic ligands are usually in the range 3–10 $M^{-1}\,cm^{-1}$, making measurement of the absorption spectrum feasible even at low (millimolar) concentrations. Another ion for which radiative lifetime can easily be determined experimentally is Eu^{III}. The emissive $^5D_0$ level deactivates to the ^7F_J multiplet and one of the transitions, $^5D_0 \rightarrow {}^7F_1$,

has pure MD character [12,13] so that it may be taken as reference [14]; as a consequence, the following equation yields $1/\tau_{rad}$ [15]:

$$A(\Psi_J, \Psi'_{J'}) = \frac{1}{\tau^{rad}} = A_{MD,0} \cdot n^3 \left(\frac{I_{tot}}{I_{MD}}\right) \quad (9)$$

The deactivation rate $A_{MD,0}$ is equal to 14.65 s^{-1} *in vacuo* and (I_{tot}/I_{MD}) is the ratio between the total integrated emission from the $Eu(^5D_0)$ level to the ^7F_J manifold (J = 0–6) and the integrated intensity of the MD transition $^5D_0 \rightarrow {}^7F_1$. The radiative lifetime can therefore be estimated from the corrected emission spectrum and the refractive index n. Three determinations of τ_{rad}, one from the experimental intrinsic quantum yield and τ_{obs} (Eq. (1)) and the two other ones from Eqs. (4)–(7) or Eq. (9), have been performed for $[Eu(dpa)_3]^{3-}$ 18–37 mM in Tris–HCl buffer (pH 7.4, dpa is dipicolinate or pyridine-2,6-dicarboxylate) and yielded τ_{rad} = 4.1, 3.15, and 4.0 ms, respectively [16]. One notes the very good agreement between the first and third values while Judd-Ofelt approach, which is more difficult to implement, results in this case in a radiative lifetime 20% too small.

2. Tailoring luminescent lanthanide complexes

The Laporte-forbidden f–f transitions have weak oscillator strengths and the excited states may be easily quenched by high-energy vibrations, such as O—H, N—H or C—H oscillators located both in the inner and outer coordination spheres. In order to achieve bright emission, a lanthanide ion needs a cleverly designed environment consisting of ligands with adequate chromophoric groups to harvest light and subsequently populate the metal–ion excited states through energy transfer, while simultaneously providing a rigid and protective coordination shell to minimize non-radiative de-activation.

2.1. Choice of the coordinating unit

Given the hard nature of lanthanide ions and therefore their preference for either ionic or ion-dipole bonding with little covalent character, adequate chelating agents contain anionic units, e.g. carboxylates, and/or O and N donor atoms, e.g. amide groups and imines. Furthermore, a survey of lanthanide coordination chemistry reveals that although Ln^{III} ions can adopt a large range of coordination numbers (CN), usually between 8 and 12 in solution and between 6 and 12 in the solid state, one of the most often encountered CN is 9. Taking these two aspects into consideration led synthetic chemists to produce a wide variety of chelating agents built up from a picolinate (pyridine-2-carboxylate) core grafted with an additional coordinating function in position 6. Three of the resulting tridentate chelating units featuring ONO or NNO donors usually react with Ln^{III} ions to yield tight and protective N_3O_6, or N_6O_3 environments around the metal ions with a coordination geometry derived from idealized tricapped trigonal prismatic (TTP, D_{3h} symmetry) environments. The tridentate units are either built in a single molecule or three of them are grafted on an anchor to yield nonadentate tripodal ligands. Typical extra functions for picolinate core are carboxylate [17,18], amide [19,20], alkylamine [21] (in this case the ligand is a tetrapodal decadentate molecule providing a N_6O_4 metal environment), or chromophoric heterocycles such as pyridine [8,22] and benzimidazole [23]. All these ligands have generated rich lanthanide coordination chemistry and can serve as building blocks to develop more elaborate polydentate ligands. In particular, two benzimidazolepyridine carboxylate units have been linked together by means of a methylene bridge to afford a class of ditopic hexadentate ligands self-assembling with lanthanide ions to form triple-stranded binuclear homo- or hetero-metallic helicates [24]. When fitted

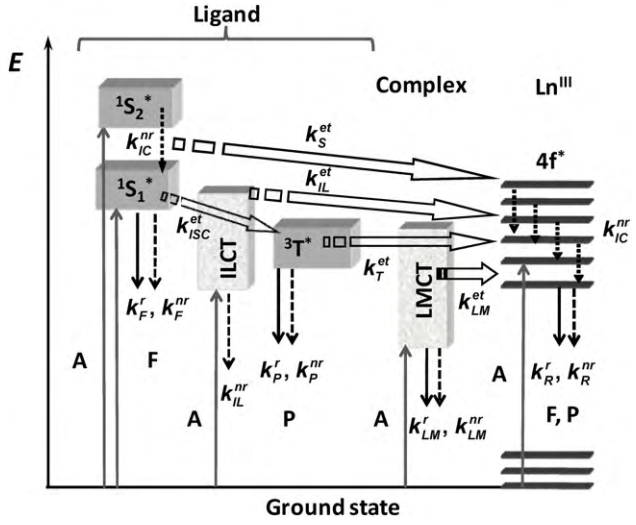

Fig. 1. Schematic representation of energy absorption, migration, emission (plain arrows) and dissipation (dotted arrows) processes in a lanthanide complex. $^1S^*$ or S = singlet state, $^3T^*$ or T = triplet state, A = absorption, F = fluorescence, P = phosphorescence, k = rate constant, r = radiative, nr = non-radiative, IC = internal conversion, ISC = intersystem crossing, ILCT (indices IL) = intra-ligand charge transfer, LMCT (indices LM) = ligand-to-metal charge transfer. Back transfer processes are not drawn for the sake of clarity.
Reproduced with permission from ref. [2]. ©The Royal Society of Chemistry, 2010.

with solubilizing hydrophilic polyoxyethylene pendant chains, the Eu^{III} and Tb^{III} helicates can be used in time-resolved luminescence imaging of live cells [25,26] and in the simultaneous detection of biomarkers expressed by cancerous tissues [27,28]. Another potential modifier group for picolinate is benzoxazole, a unit which has been tested as a chromophore to sensitize lanthanide luminescence [29] but which has not been studied much with respect to lanthanide coordination. Recently we have demonstrated the ability of this chromophore to transfer energy onto Eu^{III} with high efficacy [30]. Furthermore, we have combined the benzoxazole binding unit with 8-hydroxyquinoline to provide efficient [31] and tunable [32] sensitization of the luminescence of NIR-emitting lanthanide ions.

2.2. Choice of the sensitizer

High-yield energy transfer from the sensitizer to the metal ion will occur if a number of conditions are met which depend on the nature of the ion, the electronic structure of the donor, as well as of their relative positioning in space [33] and the nature of the interaction between them. Several levels from both the ligand and the metal ions are implied, as well as several mechanisms [34]. Donor levels are for instance singlet $^1S_i^*$ (i = 1, 2), triplet $^3T^*$, intra-ligand charger transfer (ILCT), ligand-to-metal charge transfer (LMCT), d-transition metal-to-ligand charge-transfer (^{3}MLCT), 4f–5d, and, sometimes, 4f states. Occasionally a combination of such states is operating creating a cascade of transfers terminating on the excited state of the emissive ion [35]. Note that energy is usually transferred to Ln^{III} levels with higher energy than the luminescent level; the initially populated metal–ion states then decay by fast internal conversion to the emissive level. These phenomena are illustrated in Fig. 1 but will not be discussed here in detail. The ligand geometric and electronic structure must take into account the various energy transfer paths [36–39], but molecule designers often rely on simple phenomenological rules considering solely the energy of the triplet state and emissive states [40,41]. In fact the potential donor levels of the sensitizer should be chosen such that they are reasonably above the Ln^{III} emissive state to avoid back-transfer and in close resonance with one of the higher excited 4f states. In our

case, we have chosen 8-hydroxyquinolinate for the NIR-emitting Yb^{III} ion and either benzimidazole, benzothiazole, or benzoxazole pyridine-carboxylate moieties for sensitizing Eu^{III} luminescence.

2.3. The radiative lifetime

Contrary to a belief sometimes encountered in the literature, the radiative lifetime is not a constant for a given ion. It is associated with a specific emitting level on one hand and, on the other hand, it depends on the refractive index n, see Eqs. (4), (8), and (9). Therefore, when Q_{Ln}^{Ln} is evaluated by means of Eq. (1) with a literature value of τ_{rad}, large errors may occur if the radiative lifetime used corresponds to that of a compound with different n, e.g. a value for a solid-state sample used for estimating Q_{Ln}^{Ln} in solution. For instance, referring to Eq. (9), the radiative lifetime of a complex in water ($n_{sol} = 1.33$) will be 30% longer than in the solid state ($n_{ss} \approx 1.5$); in turn this automatically means that Q_{Ln}^{Ln} and Q_{Ln}^{L} will be smaller. The latter statement is made under the assumption that the coordination sphere is the same in both media and that non-radiative de-activation processes, are similar as well. This has been recently verified for tris(dipicolinate) europium(III) [16] for which the refractive index has been measured: the solid-state sample has $\tau_{rad} = 2.6$ ms increasing to 4.1 ms for an aqueous solution, that is $2.6/4.1 = 0.63 \approx (n_{sol}/n_{ss})^3 = (1.338/1.517)^3 = 0.68$ [16].

It is crystal clear that given a coordination environment and a medium, the shorter is the radiative lifetime, the more emissive the Ln^{III} complex will be. This is in fact linked to the intrinsic properties of the f–f transitions. A highly forbidden transition, i.e. involving pure 4f orbitals, corresponds to a long radiative lifetime. If the 4f states are mixed (J-mixing for instance) or incorporate vibrational functions and/or ligand or charge transfer states, selection rules will be somewhat relaxed and the transition will be "more allowed".

Sizeable shortening of the radiative lifetime can be obtained when the luminophore is positioned in the vicinity of conducting metallic surfaces or particles such as silver islands [42–44]. The phenomenon is called metal-enhanced luminescence. The incident electric field (from the electromagnetic wave) is modified upon interacting with the metal and the result is a strong coupling between the surface plasmon polaritons in the islands and the transition dipoles of the chromophore. The radiative lifetime is substantially decreased and, in parallel, luminescence intensity is enhanced [44]. Since the effect can be generated with silver-coated nanoparticles [45], considerable applications are foreseen, for instance in bio-analyses [46,47]. This aspect is not dealt with in this review.

Therefore, one way of optimizing the design of a luminescent lanthanide complex is to have a handle on the tuning of the degree of orbital mixing and consequently on τ_{rad}. Given the inner nature of the 4f orbitals, this is by no means trivial. We note, however, that some classes of complexes such as tris or tetrakis(β-diketonates) [48] have large quantum yields despite relatively short observed lifetimes, typically on the order of 0.5–0.6 ms for $Eu(^5D_0)$ which, in turn, means that τ_{rad} must be relatively short. Similar conclusions have been presented for highly luminescent Tb^{III} complexes with 3-phenyl-4-acyl-5-isoxazolonate ($Q_{Ln}^{L} \approx 65$–75%) with short observed (0.79–0.92 ms) and radiative (0.81–0.96 ms) lifetimes [49]. Although this reasoning is relatively obvious, no systematic study has been carried out to decipher the relationship between the electronic structure of the ligand-to-metal bond and the radiative lifetime. Moreover, there are only few reliable τ_{rad} values for coordination compounds published in the literature with the exception of data for Nd^{III} and Er^{III} for which Judd-Ofelt theory works well and these values can be easily extracted from Eqs. (4)–(7) [50]; interest for these two ions lie in their incorporation into optical materials for lasers and telecommunications. It is noteworthy that radiative lifetimes may span a broad range: reported τ_{rad} values for $^5D_0$(Eu) for instance lie between 1 and 11 ms [5]. Moreover, a commonly assessed value for $^2F_{5/2}$(Yb) is 2 ms [51], but recent determinations for complexes with organic ligands show this lifetime being between 0.5 and 1.3 ms [15,16,31].

We have now started a program in our laboratories aiming at gathering reliable experimental τ_{rad} data and related photophysical parameters (Q_{Ln}^{Ln} and η_{sens}) for two of the lanthanide ions and at correlating them with structural parameters. The first ion investigated is Eu^{III} which is very important in a variety of practical applications, from phosphors for displays and lighting devices to security inks for bar codes [52] and bio-probes [28]. The second ion is Yb^{III} which presently attracts considerable interest in view of its 0.98-μm emission lying in the optical window of biological tissues and henceforth penetrating deeply into them; in the same context, it is also commonly used as activator for Er^{III} in up-converting nanoparticles [53]. In the following sections, we summarize the results obtained so far for mononuclear and binuclear Eu^{III} complexes, having a N_6O_3, N_4O_5, or N_3O_6 coordination environment, as well as for binuclear heterometallic Na^{I}–Yb^{III} complexes with N_4O_4 coordination and mononuclear Yb^{III} complexes with N_6O_3 coordination.

3. Radiative lifetimes of europium complexes

3.1. Experimental data

Chemical structures of the ligands are shown in Schemes 1 and 2, and typical molecular structures are depicted in Fig. 2. In the case of mononuclear complexes with benzothiazole- and benzoxazole-derivatized ligands, only one anhydrous tris complex was obtained, $[Eu(LO)_3]$, all the other complexes featuring two coordinated water molecules and one monodentate ligand bound through the carboxylate unit, $[Eu(L)_3(H_2O)_2]$ ($L^- = LO^-$, $LOMe^-$, LBr^-, LS^-), giving rise to a N_4O_5 coordination. On the other hand, all the benzimidazole-derivatized ligands gave anhydrous tris complexes $[Eu(Ligand)_3]$. Several crystal structures of good quality are available so that a bond valence analysis could be conducted [54,55]. In this analysis, the bond valence sum V_{Ln} defined by Eq. (10) is supposed to match the formal oxidation state of the metal ion if average bond distances are standard. Each donor atom j lying at a distance $d_{Ln,j}$ from the metal ion is characterized by a bond-valence contribution $v_{Ln,j}$:

$$V_{Ln} = \sum_j v_{Ln,j} \tag{10}$$

$$v_{Ln,j} = e^{(R_{Ln,j} - d_{Ln,j})/b} \tag{11}$$

$R_{Ln,j}$ are the bond-valence parameters for the pair of interacting atoms (Ln—O [56] or Ln—N [57]), and b is a constant equal to 0.37 Å. The bond valence sums for the mononuclear Eu^{III} complexes are in the range 2.96–3.07 (average 3.01, see Table 1) and agree well the expected value for Eu^{III} (3.00), within the variability of the method. Moreover, the average contributions from the various coordinating groups are nearly constant and are in the expected series (py = pyridine, b = benzazole): $v(CO_2^-)$, $0.41(2) > v(OH_2)$, $0.35(2) > v(N_{py})$, $0.32(2) > v(N_b)$, 0.25(4).

Together with the geometric data from the crystal structures reported [10,30], these values indicate fairly similar bonding strengths in the N_4O_5 and N_6O_3 environments of the Eu^{III} ion. In particular, comparing $[Eu(LO)_3]$ with $[Eu(LO)_3(H_2O)_2]$, the replacement of a N_{py} and a N_b coordinating atoms by O_w atoms has no significantly detectable effect on the bonding strength of the amine groups, except for a slight decrease in $v_{Ln,j}(N_{py})$, at the limit of experimental error. Since the bonding strength of O_w is larger compared to the one of the N atoms, V_{Ln} has a slightly larger value in the hydrated complex, 3.06 *vs.* 2.97. On the other hand, no difference

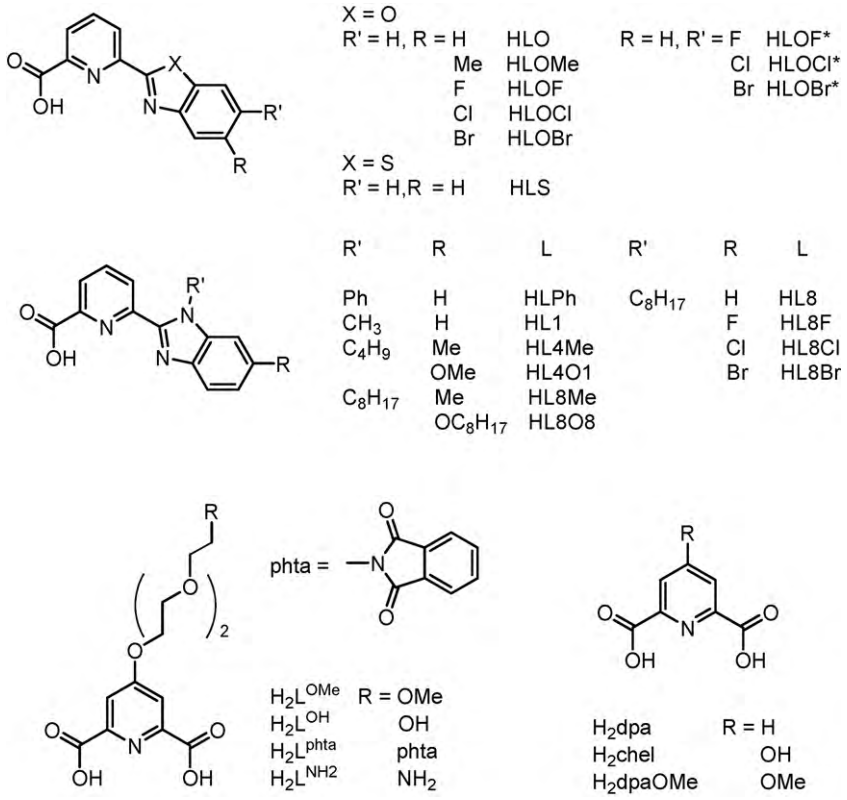

Scheme 1. Monotopic tridentate ligands [9,10,17,30].

in the bond valence parameters is observed between benzoxazole-, and benzimidazole-based anhydrous tris complexes.

The photophysical parameters for the mononuclear complexes with benzothiazole-, benzoxazole-, and benzimidazole-pyridine ligands are collected in Table 2. Analyzing data for solid-state samples of the three hydrated benzoxazole complexes with N_4O_5 coordination environment, we note that the photophysical parameters Q_{Eu}^{L} (12–14%), τ_{obs} (0.41–0.47 ms), τ_{rad} (3.2–3.5 ms), and therefore Q_{Eu}^{Eu} (12–14%) are very similar. In DMSO solution, the water ligands are replaced with stronger coordinating DMSO molecules [63]. Given the hard nature of both ligands, we however do not anticipate a large difference in orbital mixing so that in view of similar refractive indices (≈1.48 for DMSO and ≈1.5 for solid-state samples), we expect only slightly larger τ_{rad} values in DMSO, which is indeed the case: 3.6–3.7 ms. The situation for $[Eu(LS)_3(H_2O)_2]$ is a bit different, τ_{rad} in DMSO being smaller than τ_{rad} for the solid-state sample; in the absence of quantitative data on the exact nature of the species in solution [30], we cannot come up with a substantiated explanation. We observe, however, that Q_{Eu}^{Eu} in DMSO is the same for the four complexes (48–55%) and is 4-fold larger than for solid-state samples, consistent with the well-known large quenching power of water molecules. This increase is not reflected in Q_{Eu}^{L} values which are only 2.2–2.8-fold larger with, as a consequence, a 1.8–1.4-fold decrease in η_{sens} which was close to unity in the solid-state samples.

A similar analysis holds for the nine-coordinate N_6O_3 benzimidazole-based complexes. Here, however, the number of investigated ligands is larger so that the relevant parameters span a wider range. Details have been discussed in the original paper, in particular the detrimental effect of the alkoxy groups in HL4O1 and HL8O8 and of the bromine substituent in HL8Br [10]. With the exception of $[Eu(L4O1)_3]\cdot H_2O$, Q_{Eu}^{L} values for solid-state samples fall into a reasonably narrow range (52–71%) while τ_{obs} spans a range between 2.5 and 3.0 ms (2.1 ms for $[Eu(LPh)_3]\cdot 1.5H_2O$). Careful examination of the crystal structures with their extended π-stacking and H-bond networks, as well as of potential electronic effects in the substituted ligands, leads to a reasonable rationalization of the observed differences. What is remarkable, however, is that τ_{rad} values are fairly constant for the entire series of complexes: 4.2–4.7 ms (3.9 for $[Eu(L8O8)_3)]\cdot 1.5H_2O$), reflecting the similar Eu^{III} coordination environments. Intrinsic quantum yields display more variation but the smaller values (51–53%) correspond

Table 1
Bond valence parameters calculated from the crystal structures (2σ between parentheses).

Compound	V_{Ln}	$v_{Ln,j}$(O)		$v_{Ln,j}$(N)		Ref.
		CO_2^-	OH_2	N_{py}	N_b	
$[Eu(LO)_3]$	2.97	0.41(1)		0.34(3)	0.24(4)	[30]
$[Eu(LO)_3(H_2O)_2]$	3.06	0.40(2)	0.36(1)	0.30(1)	0.26(3)	[30]
$[Eu(LOMe)_3(H_2O)_2]$	3.01	0.40(4)	0.34(1)	0.31(1)	0.25(1)	[30]
$[Eu(LS)_3(H_2O)_2]$	2.96	0.41(1)	0.34(1)	0.31(1)	0.22(1)	[30]
$[Eu(L1)_3]$	3.01	0.43(1)		0.32(1)	0.25(2)	[10]
$[Eu(L4Me)_3]$	3.01	0.41(2)		0.31(1)	0.28(5)	[10]
$[Eu(L4O1)_3]$	3.05	0.41(2)		0.33(2)	0.27(7)	[10]
Averages	3.01(4)	0.41(2)	0.35(2)	0.32(2)	0.25(4)	

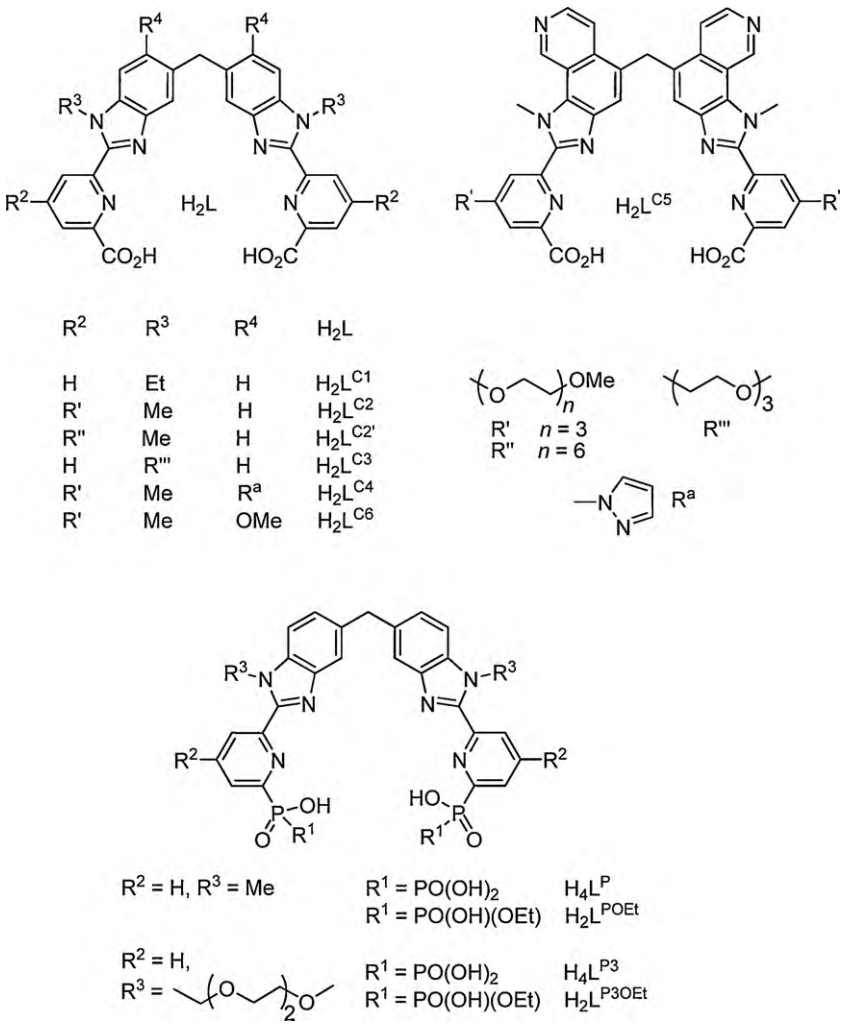

Scheme 2. Ditopic ligands with benzimidazole chromophores for the self-assembly of lanthanide binuclear helicates [25,58–60].

to complexes with co-crystallized water molecules so that one may infer a contribution from these outer-sphere molecules to the deactivation of the excited state [64]. Un-solvated complexes have Q_{Eu}^{Eu} in the range 60–68%. When the complexes are dissolved in CH_2Cl_2 ($n \approx 1.42$), one anticipates a lengthening of τ_{rad} by ≈15%, which is not observed: τ_{rad} spans a similar, although narrower, range of values compared to the solid-state samples (4.3–4.4 ms). Here one can only speculate on the origin of this discrepancy. In fact it has been recently shown that extended intermolecular interactions in crystals of Eu^{III} complexes with simple aromatic ligands influence the bonding strength of the donor atoms [35,65,66]. These interactions are destroyed in solution and when the solvent is non-coordinating, such as CH_2Cl_2 as opposed to DMSO, the inner-sphere ligands are probably more tightly bound, which would create a larger orbital mixing and therefore a shortening in τ_{rad} compensating the effect of the reduced refractive index with respect to solid-state samples.

Overall, the radiative lifetime of the solid-state N_6O_3 complexes (4.4 ± 0.4 ms, 10 samples) is about 30% larger than the radiative lifetime of the N_4O_5 complexes (3.4 ± 0.3 ms, 4 samples); can this be traced back to larger bond valence contribution of the O-donor atoms compared to N-donor atoms leading to more orbital mixing? If this assumption were correct, one should observe a similar trend for the mononuclear complexes with dipicolinate derivatives (N_3O_6) compared to the binuclear helicates (N_6O_3). Unfortunately, no valence bond analysis is available for the tris(dipicolinate) derivatives or for the binuclear helicates for which few crystal structures have been solved [62], at least for those for which detailed photophysical data are available. However, the reported luminescence spectra are fairly similar so that large differences in the bonding pattern can be excluded. The relevant photophysical parameters are listed in Table 3. With two exceptions, these data pertain to aqueous solutions in Tris–HCl buffer (pH 7.4) so that comparison between solid state and solution samples with respect to the $1/n^3$ refractive index dependence is not statistically satisfying. Nevertheless, we have already mentioned the good agreement reached for $[Eu(dpa)_3]^{3-}$ and this is also the case for the $[Eu_2(L^{C2})_3]$ helicate: $\tau_{rad}(\text{solid state})/\tau_{rad}(H_2O) = 0.71$, in perfect agreement with $(n_{sol}/n_{ss})^3 \approx (1.338/1.5)^3 = 0.71$, a result again consistent with the large similarity in the emission spectra (crystal-field splitting and relative intensities of the $^5D_0 \rightarrow {}^7F_J$ transitions).

The radiative lifetime for aqueous solutions of the mononuclear complexes with N_3O_6 coordination falls into the narrow range 3.5–4.0 ms with an average value of 3.7 ± 0.4 ms (6 samples). The intrinsic quantum yields are also much alike, between 36 and 42%, so that differences in overall quantum yields are a consequence of differences in the sensitization efficiency. When considering the binuclear helicates with carboxylate ligands H_2L^{CX} ($x = 1$–5, 2′), the same observation holds: despite very different overall quantum yields (9–24%), both τ_{obs} (2.2–2.5 ms), τ_{rad} (6.2–6.9 ms) and, consequently, Q_{Eu}^{Eu} (35–40%) can be considered as almost constant in the series. The radiative lifetime for $[Eu_2(L^{C6})_3]$ (6.8 ms), for which

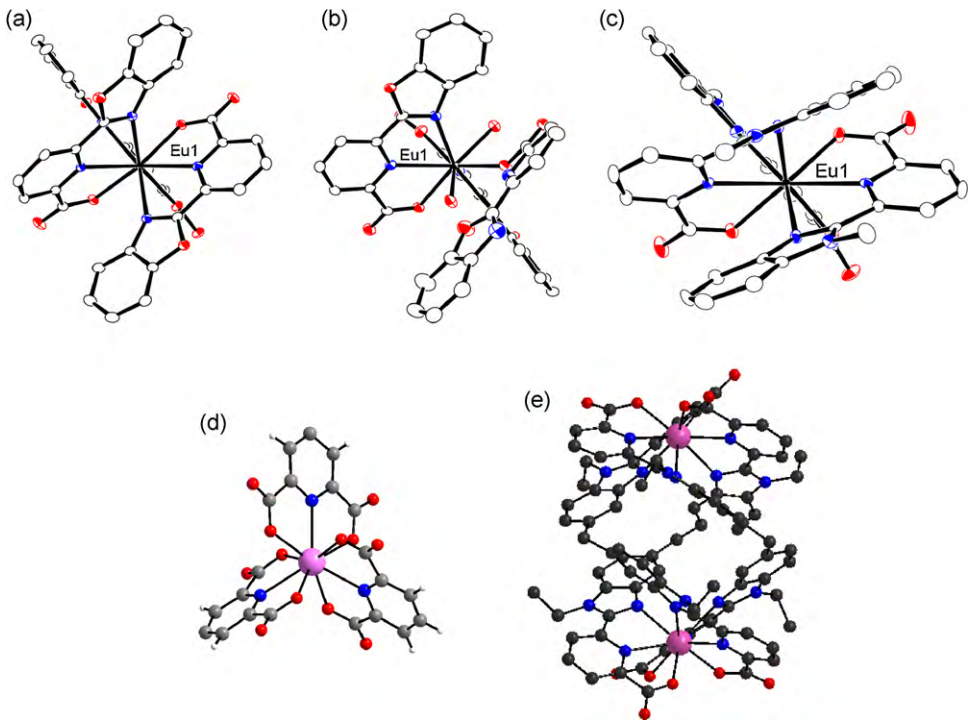

Fig. 2. Molecular structures of (a) $[Eu(LO)_3]$, (b) $[Eu(LO)_3(H_2O)_2]$ [30], (c) $[Eu(L1)_3]$ [10] (reproduced with permission, ©American Chemical Society 2009), (d) $[Eu(dpa)_3]^{3-}$ (redrawn from ref. [61]), and (e) $[Eu_2(L^{C1})_3]$ (redrawn from ref. [62]).

substantial back-energy transfer occurs [58], also falls in the above-mentioned range while τ_{obs} (0.54 ms), Q_{Eu}^{Eu} (8%), and Q_{Eu}^{L} (0.35%) are heavily affected by this detrimental process. The average value of the radiative lifetime for the helicates in aqueous solution is 6.6 ± 0.5 ms (7 samples). Again, the radiative lifetime is longer when the number of O-donor atoms is smaller in the inner coordination sphere but in contrast with the compounds listed in Table 2, the difference is much larger, +78% in going from N_3O_6 to N_6O_3

Table 2
Photophysical parameters of the mononuclear Eu^{III} complexes with benzothiazole-, benzoxazole-, and benzimidazole-pyridine ligands at room temperature.

Compound	Sample[a]	τ_{obs} (ms)	Q_{Eu}^{L} (%)	τ_{rad} (ms)[b]	Q_{Eu}^{Eu} (%)[b]	η_{sens} (%)[b]	Ref.
$[Eu(LS)_3(H_2O)_2]\cdot 2H_2O$	Solid	0.42(1)	13(2)	3.2	13	98	[30]
	DMSO	1.39(1)	29(4)	2.7	51	56	[30]
$[Eu(LO)_3(H_2O)_2]\cdot H_2O$	Solid	0.41(1)	12(2)	3.5	12	≈100	[30]
	DMSO	1.97(1)	31(5)	3.6	55	57	[30]
$[Eu(LOMe)_3(H_2O)_2]\cdot H_2O$	Solid	0.47(5)	14(2)	3.3	14	97	[30]
	DMSO	2.00(3)	39(6)	3.7	54	72	[30]
$[Eu(LOBr)_3(H_2O)_2]\cdot THF$	Solid	0.46(5)	13(2)	3.5	13	98	[30]
	DMSO	1.73(3)	29(4)	3.6	48	60	[30]
$[Eu(L1)_3]\cdot H_2O$	Solid	2.47(3)	61(2)	4.7	53	≈100	[9]
$[Eu(LPh)_3]\cdot 1.5H_2O$	Solid	2.14(1)	58(1)	4.2	51	≈100	[9]
$[Eu(L4Me)_3]\cdot 2H_2O$	Solid	2.58(1)	56(2)	4.4	58	96	[9]
$[Eu(L4O1)_3]\cdot H_2O$	Solid	2.93(2)	43(2)	4.5	65	66	[10]
$[Eu(L8)_3]$	Solid	2.95(2)	71(1)	4.6	64	≈100	[10]
	CH_2Cl_2	2.76(1)	52(1)	4.4	63	83	[10]
$[Eu(L8F)_3]$	Solid	3.00(2)	68(3)	4.4	68	100	[10]
	CH_2Cl_2	2.74(2)	51(1)	4.3	63	81	[10]
$[Eu(L8Cl)_3]$	Solid	2.94(3)	71(2)	4.4	67	≈100	[10]
	CH_2Cl_2	2.71(1)	51(2)	4.4	62	82	[10]
$[Eu(L8Br)_3]$	Solid	2.51(1)	54(1)	4.2	60	89	[10]
	CH_2Cl_2	2.73(2)	51(1)	4.3	64	80	[10]
$[Eu(L8Me)_3]\cdot 0.5H_2O$	Solid	2.69(1)	68(4)	4.4	61	≈100	[10]
	CH_2Cl_2	2.81(1)	52(1)	4.4	64	81	[10]
$[Eu(L8O8)_3]\cdot 1.5H_2O$	Solid	2.45(1)	52(4)	3.9	63	82	[10]
	CH_2Cl_2	2.39(2)	42(1)	4.4	55	77	[10]

[a] Concentrations ≈ 2×10^{-4} M in DMSO, $(6–8) \times 10^{-4}$ M in CH_2Cl_2.
[b] Q_{Eu}^{Eu}, η_{sens} and τ_{rad} calculated from Eqs. (3) and (9). For solid-state samples, $n = 1.5$ was assumed; errors on Q_{Eu}^{Eu} and η_{sens} are of the same magnitude as errors on τ_{obs} and Q_{Eu}^{L}, respectively, see refs. [9,10,30].

Table 3
Photophysical parameters of the mononuclear Eu^{III} complexes with dipicolinate derivatives and of the binuclear helicates at room temperature.

Compound	Sample[a]	τ_{obs} (ms)	Q^{L}_{Eu} (%)	τ_{rad} (ms)[b]	Q^{Eu}_{Eu} (%)[b]	η_{sens} (%)[b]	Ref.
$[Eu(dpa)_3]^{3-}$	H_2O	1.7(1)	29(2)	4.0	41	68	[16]
	Solid	1.8(1)	58(3)	2.7	68	87	[16]
$[Eu(L^{OH})_3]^{3-}$	H_2O	1.36(1)	12(2)	3.8	36	33	[17]
$[Eu(L^{OMe})_3]^{3-}$	H_2O	1.36(2)	27(4)	3.6	38	70	[17]
$[Eu(L^{NH2})_3]^{3-}$	H_2O	1.43(1)	29(4)	3.6	40	72	[17]
$[Eu(L^{Phta})_3]^{3-}$	H_2O	1.47(1)	18(3)	3.5	42	44	[17]
$[Eu(dpaOMe)_3]^{3-}$	H_2O	1.36(1)	16(2)	3.8	36	45	[17]
$[Eu_2(L^{C1})_3]$	H_2O	2.4(1)	24(3)	6.8	37	67	[25]
$[Eu_2(L^{C2})_3]$	H_2O	2.4(1)	21(2)	6.9	36	58	[67]
	Solid	2.36(1)	24(3)	4.9	48	50	This work
$[Eu_2(L^{C2'})_3]$	H_2O	2.4(1)	19(2)	6.6	37	52	[60]
$[Eu_2(L^{C3})_3]$	H_2O	2.2(1)	11(2)	6.2	36	30	[68]
$[Eu_2(L^{C4})_3]$	H_2O	2.52(2)	15(2)	6.4	40	38	[58]
$[Eu_2(L^{C5})_3]$	H_2O	2.30(2)	9(1)	6.7	35	26	[58]
$[Eu_2(L^{C6})_3]$	H_2O	0.54(2)	0.35(5)	6.8	8	4	[58]
$[Eu_2(L^{P3})_3]$	H_2O	1.9(2)	6(2)	4.2	45	13	[59]
$[Eu_2(L^{POEt})_3]$	H_2O	3.2(1)	25(2)	4.8	67	37	[59]

[a] In 0.1 M Tris–HCl buffer, pH 7.4.
[b] Q^{Eu}_{Eu}, η_{sens} and τ_{rad} calculated from Eqs. (3) and (9). For solid-state samples, $n = 1.5$ was assumed; errors on Q^{Eu}_{Eu} and η_{sens} are of the same magnitude as errors on τ_{obs} and Q^{L}_{Eu}, respectively.

coordination. Comparing the two series of complexes with N_6O_3 coordination necessitates to adjust the τ_{rad} value for the refractive index difference (≈1.5 *vs* 1.338): one finds 4.7 ± 0.4 ms for the carboxylate helicates (7 samples), which compares extremely well with 4.4 ± 0.4 ms for the benzimidazole-based mononuclear complexes (10 samples)!

The two helicates with phosphonate groups replacing carboxylate units have significantly different photophysical parameters. A detailed analysis is difficult since only two sets of data are available. The shorter radiative lifetime recorded for these complexes is, however, consistent with the larger coordination affinity of the phosphonate groups for lanthanides compared to carboxylate moieties [22] which results in helicates with H_2L^{P3} and H_2L^{POEt} having log β_{23} values larger by 1 unit compared to their carboxylate analogues [59].

3.2. Testing a potential relationship with the nephelauxetic effect

The above discussion firmly establishes a link between the radiative lifetime and the "bonding strength" in the complexes. Since τ_{rad} is influenced by orbital mixing, one may think of looking if a relationship can be found between the radiative lifetime and the nephelauxetic effect [69] because contribution of the various donor atoms to this phenomenon affects the energy of the $^5D_0 \rightarrow {}^7F_0$ transition, which can be easily measured experimentally. A phenomenological equation has been proposed by Frey and Horrocks [70] who analyzed $^5D_0 \leftarrow {}^7F_0$ excitation spectra of several Eu^{III} complexes at room temperature and came up with a series of parameters for contributing donor atoms and groups. In view of the very small Stokes' shift in f–f transitions (1–2 cm^{-1}), either excitation or emission spectra can be used for this purpose. When experimental data are recorded at low temperature a correction of 1 cm^{-1}/24 K can be applied to estimate the value at room temperature. The relationship is as follows:

$$\tilde{\nu}_{0-0}\,[cm^{-1}] = 17\,374 + C\sum_i n_i \cdot \delta_i \qquad (12)$$

where 17 374 cm^{-1} is the value for gaseous Eu^{III} calculated from energy matrices taking into account electrostatic and spin–orbit interactions [71]; C is a coefficient depending on the coordination number ($C = 1.0$ for CN = 9), δ_i is the nephelauxetic effect generated by each coordinating atom or group, and n_i is the number of such groups in the inner coordination sphere. Initial values for C and δ_i were determined from a set of 37 Eu^{III} complexes. For the coordinating groups of interest here and CN = 9, the nephelauxetic parameters are $\delta_{carb} = -17.2\ cm^{-1}$ for the carboxylate, $\delta_w = -10.4\ cm^{-1}$ for water, and $\delta_N = -12.1\ cm^{-1}$ for imine nitrogen atoms [70]. Subsequently, we have shown that for the heterocyclic nitrogen atoms of benzimidazolepyridines, a more adequate value is $\delta_{bzp} = -15.3\ cm^{-1}$ [72]. The relationship has to be used with care in that the nephelauxetic effect will depend on the Ln-donor atom distance and, more generally, on the electron density on the donor atoms. For instance, the nephelauxetic parameters of the pyridine and benzimidazole N atoms in trinuclear and tetranuclear helicates have been found to be substantially different, −25.3 and −8.0 cm^{-1}, respectively [73], a fact substantiated by NMR data and in line with the larger capacity of pyridine rings to expand their electronic clouds [74]; however, the average value (−16.6 cm^{-1}) is close to −15.3 cm^{-1}. Using the latter parameter, $\tilde{\nu}_{calc}$ values have been estimated for the N_3O_6, N_4O_5, and N_6O_3 chemical environments described here and are compared in Table 4 with the few available experimental data. Phenomenological Eq. (12) yields satisfying results for the N_3O_6 and N_6O_3 coordination environments but the only available experimental value for the N_4O_5 environments shows large discrepancy with the calculated value. This may be due to the water molecules being involved in H-bonding

Table 4
Energy (cm^{-1}) of the $Eu(^5D_0 \rightarrow {}^7F_0)$ transitions at room temperature as estimated from Eq. (12) and found experimentally, as well as radiative lifetime of the $Eu(^5D_0)$ level for solid-state samples.

	$\tilde{\nu}_{calc}$ (cm^{-1})	$\tilde{\nu}_{obs}$ (cm^{-1})	Compnds	Sample	Refs.	τ_{rad} (ms)
N_4O_5	17 240	17 269	$[Eu(LOMe)_3(H_2O)_2]$	Solid	[30]	3.3
N_6O_3	17 231	17 236(4)	7 Carboxylate helicates	H_2O	[25,58,60]	4.7(4)[a]
N_3O_6	17 225	17 232	$[Eu(dpa)_3]^{3-}$	Solid	[70]	2.7

[a] Recalculated from solution data with $n = 1.5$.

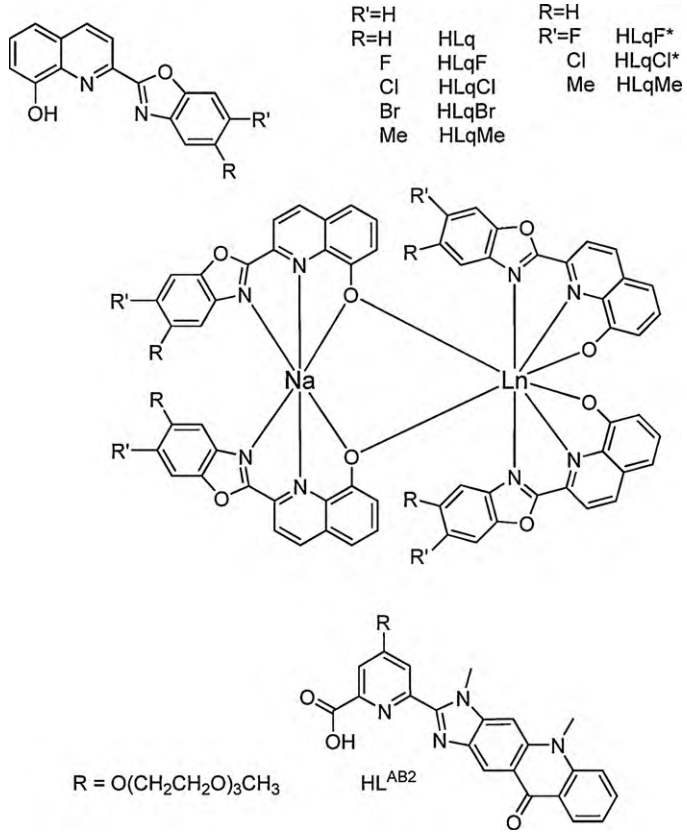

Scheme 3. 8-Hydroxyquinoline ligands for heteronuclear Yb^{III} complexes [31] and picolinic acid fitted with a fused acridone/benzimidazole substituent [75].

resulting in weakened Eu—OH_2 bonds and points to subtle effects potentially having large influence on $\tilde{\nu}_{0-0}$. Data reported in Table 4 unravel a qualitative relationship between τ_{rad} and $\tilde{\nu}_{0-0}$ when comparing either N_3O_6 and N_6O_3 or N_3O_6 and N_4O_5 coordination environments, in that a larger nephelauxetic effect (i.e. smaller $\tilde{\nu}_{0-0}$) corresponds to a smaller value of the radiative lifetime. But this trend is reverse when comparing N_6O_3 with N_4O_5 coordination. Therefore more experimental data are obviously needed to test if τ_{rad} can effectively be correlated with the nephelauxetic effect as measured via the energy of the Eu($^5D_0$) level.

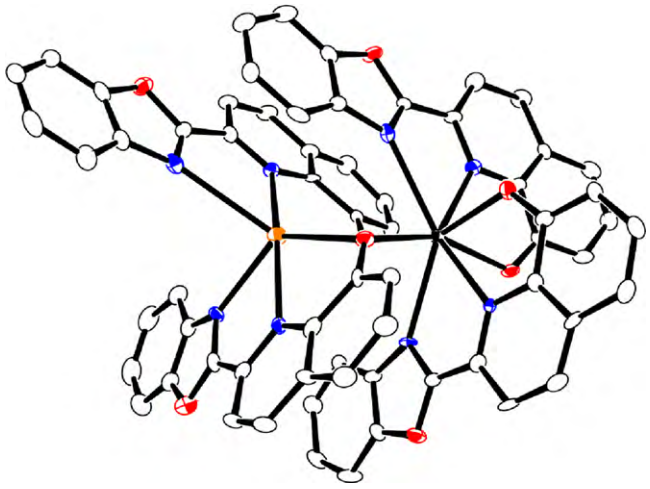

Fig. 3. Molecular structure of [NaYb(Lq)$_4$].
Reproduced with permission from ref. [31]. ©American Chemical Society 2009.

4. Radiative lifetimes of ytterbium complexes

Most of the Yb^{III} complexes for which radiative lifetimes could be determined experimentally are binuclear Na^I–Yb^{III} compounds obtained upon reaction of the benzoxazole-8-hydroxyquinoline ligands HLqX (Scheme 3) with ytterbium chloride in presence of sodium hydroxide and in which Yb^{III} is eight-coordinate. A typical structure is shown in Fig. 3. Bond-valence analysis conducted on five X-ray structures evidenced close similarity in the bonding pattern and the bond valence parameters found for O(CO_2^-), 0.43(2), and N_b, 0.23(2), are identical, within experimental errors, to those listed in Table 1 for the Eu^{III} complexes. Other investigated complexes are nine-coordinate [Yb(dpa)$_3$]$^{3-}$ and [Yb(L^{AB2})$_3$] (Scheme 3).

Yb^{III} only possesses two 4f levels and the emissive $^2F_{5/2}$ level is located 10 200 cm^{-1} above the $^2F_{7/2}$ ground state. Several excitation mechanisms have been proposed but will not be discussed here [51]. The relatively small energy gap between the emissive and receiving levels can be easily bridged by high energy vibrations such as C—H, N—H, or O—H, so that reported quantum yields for Yb^{III} complexes with organic ligands are usually small, in the range 0.5–4%. In fact, the quantum yields for the binuclear [NaYb(LqX)$_4$] complexes listed in Table 5 are, to our knowledge, among the largest ones reported so far for complexes with organic ligands. With the

Table 5
Photophysical parameters of the Yb^{III} complexes at room temperature.

Compound	Sample	τ_{obs} (μs)	Q^L_{Yb} (%)	τ_{rad} (μs)[a]	Q^{Yb}_{Yb} (%)[b]	η_{sens} (%)[b]	Ref.
[NaYb(Lq)$_4$]·H_2O	Solid	19	3.1	623	3.0	≈100	[31]
[NaYb(LqF)$_4$]	Solid	20	3.3	635	3.1	≈100	[31]
[NaYb(LqCl)$_4$]·(H_2O)$_{0.5}$	Solid	19	3.2	594	3.2	≈100	[31]
[NaYb(LqBr)$_4$]·(H_2O)$_{0.5}$	Solid	18	3.0	632	2.9	≈100	[31]
[NaYb(LqMe)$_4$]	Solid	22	3.7	603	3.6	≈100	[31]
[NaYb(LqF*)$_4$]·H_2O	Solid	10	1.9	513	1.9	≈100	[31]
	CH_2Cl_2	20	2.4	745	2.7	≈100	[31]
[NaYb(LqCl*)$_4$]	Solid	20	3.4	571	3.5	≈100	[31]
[NaYb(LqMe*)$_4$]	Solid	22	3.6	629	3.5	≈100	[31]
	CH_2Cl_2	20	2.6	706	2.8	≈100	[31]
[Yb(L^{AB2})$_3$]	Solid	24.8	1.6	830	3.0	54	[75]
	$CHCl_3$/MeOH	16.5	1.1	900	1.8	61	[75]
Na_3[Yb(dpa)$_3$]	H_2O[c]	2.23	0.015	1310	0.2	8	[16]

[a] τ_{rad} determined from Eq. (8) for solutions; for solid-state samples, calculated from solution value with adjustment for the refractive index, assuming $n = 1.5$.
[b] Q^{Yb}_{Yb} and η_{sens} calculated from Eqs. (1) and (3); errors on Q^{Yb}_{Yb} and η_{sens} are of the same magnitude as the errors on τ_{obs} and Q^L_{Yb}, respectively, see ref. [31].
[c] In 0.1 M Tris–HCl buffer, pH 7.4; concentration 4×10^{-2} M.

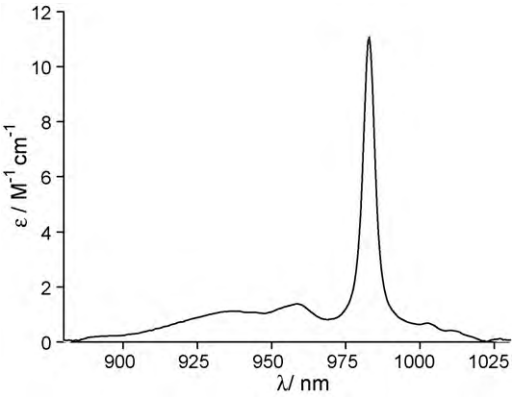

Fig. 4. Near-infrared absorption spectrum of $[NaYb(LqMe^*)_4]$ 8.4×10^{-4} M in CH_2Cl_2.
Redrawn from ref. [31].

exception of the hydrated complex with HLqF* for which the co-crystallized water molecule is H-bonded to a ligand and lies at a short distance from the metal ion (4.5 Å), the solid-state samples of the $[NaYb(LqX)_4]$ complexes have remarkably similar values of τ_{obs} (18–22 μs, average 20(3) μs) and Q_{Yb}^{L} (3.0–3.6%, average 3.3(0.5)%). Radiative lifetimes have been determined experimentally for solutions of the complexes with $HLqF^*$ and $HLqMe^*$ in methylene chloride by means of Eq. (8); a typical absorption spectrum is reported in Fig. 4. The radiative lifetimes for the solid-state samples have been calculated with the help of Eqs. (1) and (3) assuming the same sensitization efficiency as for the solutions (100%). We note that in the case of $[NaYb(LqMe^*)_4]$, for which both solid state and solution data are available, the ratio between the radiative lifetimes, 0.89, is close to the expected value of 0.90 calculated on the basis of the refractive index correction according to Eq. (8). Again with the exception of $[NaYb(LqF^*)_4]$, the radiative lifetimes of the solid-state samples span a relatively narrow range, 571–635 μs (average: 612(48) μs) and consequently, Q_{Yb}^{Yb} values are very similar. Regarding the solutions in CH_2Cl_2, the observed lifetimes are equal to the average found for solid-state samples while the ligand-sensitized quantum yields are smaller by about 25%; this is entirely due to smaller values of Q_{Yb}^{Yb} arising from longer radiative lifetimes.

In going from the N_4O_4 coordination environment in the binuclear complexes to a N_6O_3 one in $[Yb(L^{AB2})_3]$ and to a N_3O_6 one in $[Yb(dpa)_3]^{3-}$, the average radiative lifetime of the solid-state samples increases from 612 to 830 and 929 μs (corrected for the refractive index). If one understands the increase between eight- and nine-coordinate complexes, the larger τ_{rad} exhibited by $[Yb(dpa)_3]^{3-}$ does not match the trend observed for the Eu^{III} complexes.

5. Conclusion

Photophysical data relevant to the sensitization of the luminescence of 29 nine-coordinate Eu^{III} and 10 eight- and nine-coordinate Yb^{III} complexes having N_xO_y coordination environments have been analyzed with respect to the radiative lifetime of the emissive state. The dependence of this parameter on the refractive index is clearly substantiated when comparing solid state and solution data. To our knowledge this is the first such compilation of τ_{rad} data for these two ions. From this study, it appears that the radiative lifetime, which is linked to the amount of orbital mixing sustained by the emissive and ground-state 4f levels, depends on the coordination environment that is on the bonding pattern in the complexes. In the case of $Eu(^5D_0)$, experimental values range from 2.7 to 6.9 ms (in all media). A tentative relationship with the nephelauxetic effect has been explored but did not yield unambiguous results. More experimental data are evidently required in order to develop a better picture of the relationship between the radiative lifetime and the *electronic* structure of the complexes. Of course, symmetry is an important parameter too in that the degree of symmetry and the presence or absence of inversion centre will influence orbital mixing to a large extent. However here, we are dealing with series of compounds having very similar coordination environments with site symmetry which is often low in the solid state, thus allowing maximum orbital mixing, although they are commonly described as deriving from higher idealized (trigonal) symmetry.

These considerations also apply to the radiative lifetime of the $Yb(^2F_{5/2})$ level, which also shows dependence on the coordination environment; the ratio between the shorter (0.5 ms) and the longer (1.3 ms) radiative lifetimes recorded is approximately the same as for $Eu(^5D_0)$, a factor 2.5. Consequently, it is clear that estimates of the intrinsic quantum yield based on the observed lifetime and a "literature value" of τ_{rad} equal to 2 ms for Yb^{III}, as often assumed by authors (see ref. [51] for a compilation) are most probably wrong. For solutions in water a value between 1.2 and 1.3 ms is more adequate, as shown by the recent determination of τ_{rad} for $[Yb(dtpa)]^{2-}$ (1.2 ms [15]). Smaller values appear to prevail in methylene chloride (0.7–0.75 ms) but here again, more experimental data are needed.

Identification of the radiative lifetime as a key parameter in the design of highly luminescent lanthanide-containing complexes is unmistakably a new way of looking at ligand engineering but a large theoretical effort is still needed before a clear connection between this parameter and the electronic structure of the complexes can be established.

Acknowledgments

This research is supported through a grant from the Swiss National Science Foundation (200020-107449/1). JCB and HKK thank the Science Foundation of Korea, Ministry of Education, Science, and Technology, for a grant within the frame of the World Class University program (grant Nr R31-10035). We are grateful to Professor Claude Piguet (University of Geneva, Switzerland) and Dr Nail Shavaleev for helpful discussions.

References

[1] J.-C.G. Bünzli, Chem. Lett. 38 (2009) 104.
[2] S.V. Eliseeva, J.-C.G. Bünzli, Chem. Soc. Rev. 39 (2010) 189.
[3] J.H. Van Vleck, J. Phys. Chem. 41 (1937) 67.
[4] B.M. Walsh, in: B. Di Bartolo, O. Forte (Eds.), Advances in Spectroscopy for Lasers and Sensing, Springer Verlag, Berlin, 2006, p. 403.
[5] J.-C. G. Bünzli, S.V. Eliseeva, in: P. Hänninen, H. Härmä (Eds.), Springer Series on Fluorescence, Lanthanide Spectroscopy, Materials, and Bio-applications, Springer Verlag, Berlin, 2010 (Chapter 2), in press.
[6] S.W.M. Shionoya, Yen in Phosphor Handbook, CRC Press Inc., Boca Raton, FL 33431, USA, 1999.
[7] O.L. Malta, H.F. Brito, J.F.S. Menezes, F.R. Gonçalves e Silva, C.D. Donega, S. Alves, Chem. Phys. Lett. 282 (1998) 233.
[8] G.S. Kottas, M. Mehlstaubl, R. Froehlich, L. De Cola, Eur. J. Inorg. Chem. (2007) 3465.
[9] N.M. Shavaleev, R. Scopelliti, F. Gumy, J.-C.G. Bünzli, Inorg. Chem. 48 (2009) 5611.
[10] N.M. Shavaleev, S.V. Eliseeva, R. Scopelliti, J.-C.G. Bünzli, Chem. Eur. J. 15 (2009) 10790.
[11] C. Görller-Walrand, K. Binnemans, in: K.A. Gschneidner Jr., L. Eyring (Eds.), Handbook on the Physics and Chemistry of Rare Earths, vol. 25, Elsevier Science B.V., Amsterdam, 1998, p. 101 (Vol. 25, Chapter 167).
[12] C. Görller-Walrand, L. Fluyt, A. Ceulemans, W.T. Carnall, J. Chem. Phys. 95 (1991) 3099.
[13] W.T. Carnall, P.R. Fields, K. Rajnak, J. Chem. Phys. 49 (1968) 4412.
[14] C. Görller-Walrand, L. Fluyt, in: K.A. Gschneidner Jr., J.-C.G. Bünzli, V.K. Pecharsky (Eds.), Handbook on the Physics and Chemistry of Rare Earths, Elsevier Science B.V., Amsterdam, 2010, p. 1 (Vol. 40, Chapter 244).

[15] M.H.V. Werts, R.T.F. Jukes, J.W. Verhoeven, Phys. Chem. Chem. Phys. 4 (2002) 1542.
[16] A. Aebischer, F. Gumy, J.-C.G. Bünzli, Phys. Chem. Chem. Phys. 11 (2009) 1346.
[17] A.-L. Gassner, C. Duhot, J.-C.G. Bünzli, A.-S. Chauvin, Inorg. Chem. 47 (2008) 7802.
[18] A. D'Aleo, A. Picot, A. Beeby, J.A. Gareth Williams, B. Le Guennic, C. Andraud, O. Maury, Inorg. Chem. 47 (2008) 10258.
[19] J.J. Lessmann, W.deW. Horrocks Jr., Inorg. Chem. 39 (2000) 3114.
[20] J.-M. Senegas, G. Bernardinelli, D. Imbert, J.-C.G. Bünzli, P.-Y. Morgantini, D.J. Weber, C. Piguet, Inorg. Chem. 42 (2003) 4680.
[21] N. Chatterton, Y. Bretonniere, J. Pecaut, M. Mazzanti, Angew. Chem. Int. Ed. 44 (2005) 7595.
[22] S. Comby, D. Imbert, A.-S. Chauvin, J.-C.G. Bünzli, L.J. Charbonnière, R.F. Ziessel, Inorg. Chem. 43 (2004) 7369.
[23] N. André, T.B. Jensen, R. Scopelliti, D. Imbert, M. Elhabiri, G. Hopfgartner, C. Piguet, J.-C.G. Bünzli, Inorg. Chem. 43 (2004) 515.
[24] C. Piguet, J.-C.G. Bünzli, in: K.A. Gschneidner Jr., J.-C.G. Bünzli, V.K. Pecharsky (Eds.), Handbook on the Physics and Chemistry of Rare Earths, Elsevier Science B.V., Amsterdam, 2010, p. 351 (Vol. 40, Chapter 247).
[25] J.-C.G. Bünzli, A.-S. Chauvin, C.D.B. Vandevyver, B. Song, S. Comby, Ann. N. Y. Acad. Sci. 1130 (2008) 97.
[26] B. Song, C.D.B. Vandevyver, A.-S. Chauvin, J.-C.G. Bünzli, Org. Biomol. Chem. 6 (2008) 4125.
[27] B. Song, V. Sivagnanam, C.D.B. Vandevyver, I.A. Hemmilä, H.-A. Lehr, M.A.M. Gijs, J.-C.G. Bünzli, Analyst 134 (2009) 1991.
[28] V. Fernandez-Moreira, B. Song, V. Sivagnanam, A.-S. Chauvin, C.D.B. Vandevyver, M.A.M. Gijs, I.A. Hemmila, H.-A. Lehr, J.-C.G. Bünzli, Analyst 135 (2010) 42.
[29] P. Thakur, V. Chakravortty, K.C. Dash, Indian J. Chem. A 38 (1999) 1223.
[30] N.M. Shavaleev, R. Scopelliti, F. Gumy, J.-C.G. Bünzli, Inorg. Chem. 48 (2009) 6178.
[31] N.M. Shavaleev, R. Scopelliti, F. Gumy, J.-C.G. Bünzli, Inorg. Chem. 48 (2009) 7937.
[32] N.M. Shavaleev, R. Scopelliti, F. Gumy, J.-C.G. Bünzli, Inorg. Chem. 48 (2009) 2908.
[33] G. Zucchi, R. Scopelliti, J.-C.G. Bünzli, J. Chem. Soc., Dalton Trans. (2001) 1975.
[34] G.F. de Sá, O.L. Malta, C.D. Donega, A.M. Simas, R.L. Longo, P.A. Santa-Cruz, E.F. da Silva, Coord. Chem. Rev. 196 (2000) 165.
[35] L.N. Puntus, K.A. Lyssenko, I. Pekareva, J.-C.G. Bünzli, J. Phys. Chem. B 113 (2009) 9265.
[36] M.K. Nah, S.G. Rho, H.K. Kim, J.G. Kang, J. Phys. Chem. A 111 (2007) 11437.
[37] M.K. Nah, J.B. Oh, H.K. Kim, K.H. Choi, Y.R. Kim, J.G. Kang, J. Phys. Chem. A 111 (2007) 6157.
[38] N.S. Baek, Y.H. Kim, Y.K. Eom, J.H. Oh, H.K. Kim, A. Aebischer, F. Gumy, A.-S. Chauvin, J.-C.G. Bünzli, Dalton Trans. 39 (2010) 1532.
[39] S.G. Roh, N.S. Baek, Y.H. Kim, H.K. Kim, Bull. Kor. Chem. Soc. 28 (2007) 1249.
[40] M. Latva, H. Takalo, V.M. Mukkala, C. Matachescu, J.-C. Rodriguez-Ubis, J. Kankare, J. Lumin. 75 (1997) 149.
[41] A.P.S. Samuel, J. Xu, K.N. Raymond, Inorg. Chem. 48 (2009) 687.
[42] J.R. Lakowicz, Anal. Biochem. 337 (2005) 171.
[43] C.D. Geddes, J.R. Lakowicz, J. Fluoresc. 12 (2002) 121.
[44] D.A. Weitz, S. Garoff, C.D. Hanson, T.J. Gramila, J.I. Gersten, Opt. Lett. 7 (1982) 89.
[45] F. Xie, M.S. Baker, E.M. Goldys, J. Phys. Chem. B 110 (2006) 23085.
[46] P. Muthu, N. Calander, I. Gryczynski, Z. Gryczynski, J.M. Talent, T. Shtoyko, I. Akopova, J. Borejdo, Biophys. J. 95 (2008) 3429.
[47] J. Zhang, E. Matveeva, I. Gryczynski, Z. Leonenko, J.R. Lakowicz, J. Phys. Chem. B 109 (2005) 7969.
[48] K. Binnemans, in: K.A. Gschneidner Jr., J.-C.G. Bünzli, V.K. Pecharsky (Eds.), Handbook on the Physics and Chemistry of Rare Earths, Elsevier Science B.V., Amsterdam, 2005, p. 107 (Vol. 35, Chapter 225).
[49] S. Biju, M.L.P. Reddy, A.H. Cowley, K.V. Vasudevan, J. Mater. Chem. 19 (2009) 5179.
[50] L.D. Carlos, R.A.S. Ferreira, V.D. Bermudez, S.J.L. Ribeiro, Adv. Mater. 21 (2009) 509.
[51] S. Comby, J.-C.G. Bünzli, in: Handbook on the Physics, Chemistry of Rare Earths, K.A. Gschneidner Jr., J.-C.G. Bünzli, V.K. Pecharsky (Eds.), Handbook on the Physics and Chemistry of Rare Earths, Elsevier Science B.V., Amsterdam, 2007, p. 217 (Vol. 37, Chapter 235).
[52] D.F. Reardon, US Patent 2008305243 A1 20081211 (2008).
[53] D.E. Cooper, A. D'Andrea, G.W. Faris, B. MacQueen, W.H. Wright, in: J.M. Van Emon (Ed.), Immunoassay and Other Bioanalytical Techniques, CRC Press, Taylor & Francis Group, Boca Raton, 2007, p. 217 (Chapter 9).
[54] I.D. Brown, Chem. Rev. 109 (2009) 6858.
[55] I.D. Brown, Acta Cryst. B 48 (1992) 553.
[56] A. Trzesowska, R. Kruszynski, T.J. Bartczak, Acta Cryst. B 60 (2004) 174.
[57] A. Trzesowska, R. Kruszynski, T.J. Bartczak, Acta Cryst. B 61 (2005) 429.
[58] E. Deiters, B. Song, A.-S. Chauvin, C. Vandevyver, J.-C.G. Bünzli, Chem. Eur. J. 15 (2009) 885.
[59] A.-S. Chauvin, S. Comby, M. Baud, C. De Piano, C. Duhot, J.-C.G. Bünzli, Inorg. Chem. 48 (2009) 10687.
[60] E. Deiters, B. Song, A.-S. Chauvin, C.D.B. Vandevyver, J.-C.G. Bünzli, New J. Chem. 32 (2008) 1140.
[61] P.A. Brayshaw, J.-C.G. Bünzli, P. Froidevaux, J.M. Harrowfield, Y. Kim, A.N. Sobolev, Inorg. Chem. 34 (1995) 2068.
[62] M. Elhabiri, R. Scopelliti, J.-C.G. Bünzli, C. Piguet, J. Am. Chem. Soc. 121 (1999) 10747.
[63] J.-C.G. Bünzli, C. Mabillard, J.-R. Yersin, Inorg. Chem. 21 (1982) 4214.
[64] A. Beeby, I.M. Clarkson, R.S. Dickins, S. Faulkner, D. Parker, L. Royle, A.S. de Sousa, J.A.G. Williams, M. Woods, J. Chem. Soc., Perkin Trans. 2 (1999) 493.
[65] L.N. Puntus, K.A. Lyssenko, M.Y. Antipin, J.-C.G. Bünzli, Inorg. Chem. 47 (2008) 11095.
[66] L.N. Puntus, Helv. Chim. Acta 92 (2009) 2552.
[67] A.-S. Chauvin, S. Comby, B. Song, C.D.B. Vandevyver, J.-C.G. Bünzli, Chem. Eur. J. 14 (2008) 1726.
[68] A.-S. Chauvin, S. Comby, B. Song, C.D.B. Vandevyver, J.-C.G. Bünzli, Chem. Eur. J. 13 (2007) 9515.
[69] C.K. Jorgensen, Prog. Inorg. Chem. 4 (1962) 73.
[70] S.T. Frey, W.deW. Horrocks Jr., Inorg. Chim. Acta 229 (1995) 383.
[71] G.S. Ofelt, J. Chem. Phys. 38 (1963) 2171.
[72] C. Piguet, J.-C.G. Bünzli, G. Bernardinelli, G. Hopfgartner, S. Petoud, O. Schaad, J. Am. Chem. Soc. 118 (1996) 6681.
[73] N. Dalla-Favera, J. Hamacek, M. Borkovec, D. Jeannerat, F. Gumy, J.-C.G. Bünzli, G. Ercolani, C. Piguet, Chem. Eur. J. 14 (2008) 2994.
[74] S. Torelli, S. Delahaye, A. Hauser, G. Bernardinelli, C. Piguet, Chem. Eur. J. 10 (2004) 3503.
[75] E. Deiters, F. Gumy, J.-C.G. Bünzli, Eur. J. Inorg. Chem. (2010), Published on the web February 10, 2010, doi:10.1002/ejic.200901148.